First-principles study of sulfur isotope fractionation in pyrite-type disulfides

Revision 2 Shanqi Liu[1], Yongbing Li[1*], Jianming Liu[2], Yaolin Shi[1]

1 Key Laboratory of Computational Geodynamics, University of Chinese Academy of Sciences, Beijing, 100049, China

2 Key Laboratory of Mineral Resources, Institute of Geology and Geophysics, Chinese Academy of Sciences, Beijing, 100029, China

Abstract The sulfides are an important group of minerals. As a geochemical tracer , the sulfur isotope fractionation in sulfides can be used to analyze the ore-forming process and the ore-forming material source . Fe, Co, Ni and Mn are the first row transition metal, and pyrite (FeS_2), cattierite (CoS_2), vaesite (NiS_2) and hauerite (MnS_2) crystallize in the pyrite-type structure. However, there are few studies on the sulfur isotope fractionation in these disulfides. So studying the isotope fractionation between them provide the opportunity to examine the various members of a structural group in which only the metal atom is changed, thereby providing information that permits a systematic development of concepts regarding sulfur isotope fractionation in transition-metal disulfides. In the present paper, the sulfur isotope fractionation parameters for pyrite, cattierite, vaesite, and hauerite with the pyrite-type structure have been calculated using first-principles methods based on density-functional theory in the temperature range of 0-1000ºC. The structure parameters of these four minerals, and the vibration frequencies of pyrite are in good agreement with previous experimental values. The metal-sulfur distance increases in the order FeS_2, CoS_2, NiS_2

* Corresponding author. Tel.: +86 010 88256476
E-mail address: yongbingli@ucas.ac.cn

and MnS_2, the sulfur-sulfur distance decreases in the order FeS_2, CoS_2, MnS_2 and NiS_2, these two sequences agree with the experimental results. Our calculations show that the order of heavy isotope enrichment is pyrite > cattierite > vaesite > hauerite. It seems that the sulfur isotope fractionation in disulfides depends mainly on the metal-sulfur bonds.

Keywords: Sulfur isotope fractionations; disulfides; pyrite; First-principles; DFPT

Introduction

Sulfides have great economic importance as the major source of most of metals. Among them, pyrite is the most abundant metal sulfide mineral in nature and occurs in a wide range of geological environments (metallic mineral deposits , sedimentary rocks, metamorphic rocks, granite, basic-ultrabasic magmatic rocks and pyrolite) (Craig and Vaughan, 1981; Wang et al. 1989; Vaughan et al. 1991). The pyrite structure, based on NaCl structure, is common to a complete series of first row transition metal disulfides extending from Mn to Zn (Temmerman et al., 1993). This family of minerals exhibits a fascinating diversity in structural chemistry, electrical, magnetic, and other physical properties (Wuensch and Ribbe, 1974; Vaughan and Craig, 1978). So studying the sulfur isotope fractionation of pyrite (FeS_2), cattierite (CoS_2), vaesite (NiS_2) and hauerite (MnS_2), which crystallize in the pyrite-type structure, may provide the opportunity to examine the various members of a structural group in which only the metal atom is changed, thereby providing information that permits a systematic development of concepts regarding sulfur isotope fractionation in transition-metal sulfides.

Since the work of Urey and Greiff (1935) and Urey (1947) on isotopic exchange equilibria and the thermodynamic properties of substances, using stable isotope fractionations to estimate the temperature of minerals formation in geochemical systems has been well established by experiment and theoretical calculation. And the rapid development of new analytical techniques provide an excellent opportunity to increase the scope of isotope geochemistry: the emergence of 'nontraditional' stable isotopes of metals, the invention of clumped isotope geochemistry, new capabilities for measurements of position-specific isotope effects in organic compounds , and a great expansion of mass-independent isotope geochemistry (Eiler et al., 2014). For sulfur element, it has four stable isotopes, ^{32}S, ^{33}S, ^{34}S and ^{36}S with an average abundance of 95.02, 0.75, 4.21, and 0.02%, respectively (Macnamara and Thode, 1950), and in the last decade, multiple sulphur isotopes have become a hot topic of research (Farquhar et al., 2003; Otake et al., 2008; Danielache et al., 2008; Balan et al., 2009; Guy et al., 2012; Halevy, 2013). And the recent study in determining the $\delta^{33}S$ and $\delta^{36}S$ values of terrestrial samples has stemmed from the finding by Farquhar et al. (2000) that some sulfide and sulfate minerals in sedimentary rocks older than ~2.0 Ga do not fall on the mass-dependent fractionation lines; this abnormal fractionation is termed "mass independent sulfur isotope fractionations (S-MIF)." However, the isotopic effects of the various mechanisms suggested to generate S-MIF are unclear, major theoretical and experimental efforts will be required to understand them (Eiler et al., 2014). For these, this study only deals with the sulfur mass dependent sulfur isotope fractionations.

As for sulfides, the complexities of the sulfide system and the difficulty in making experiments on sulfur isotopic fractionations between sulfides make the studies on sulfur isotope fractionation in sulfides relatively weak. So far, the experimental researches, which aim at sulfur isotope fractionations in sulfides, have focused on a few minerals, such as ZnS, PbS, FeS_2, $CuFeS_2$, CuS, CuS_2, AgS and Bi_2S_3 (Grootenboer and Schwarcz, 1969; Kajiwara et al., 1969; Rye and Czamanske, 1969; Czamanske and Rye, 1974; Kajiwara and Krouse, 1971; Salomons, 1971; Kiyosu, 1973; Smith et al., 1977; Hubberten, 1980; Bente and Nielsen, 1982). And the theoretical calculations of sulfur isotope fractionation are also few. Sakai (1968) used Debye-Einstein model calculating the isotopic properties of sulfur compounds in hydrothermal processes; Hulston (in Groves et al., 1970) also used Debye-Einstein model calculating the reduced partition function ratios (β-factors) of ZnS and PbS; Elcombe and Hulston (1975) obtained the sulfur isotope fractionation between ZnS and PbS by lattice dynamical model; Li and Liu (2006) calculated the sulfur isotope fractionation of ZnS, PbS, $FeCuS_2$, FeS, CdS, Cu_5FeS_4, Cu_3VS_4, $CuFe_2S_3$ and $FeNi_2S_4$ over a temperature range from 0 ºC to 1000 ºC using the modified increment method; Blanchard et al. (2009) computed the sulfur isotope fractionation of FeS_2, ZnS and PbS using first-principles density functional method.

In this paper, we use first-principles calculations based on density functional theory to calculate the reduced partition function ratios of pyrite-type FeS_2, CoS_2, NiS_2 and MnS_2 as a function of temperature.

Calculation methods

In the present study, sulfur isotope fractionation is assumed to be mass dependent, driven by changes in vibrational energies in crystals (Urey, 1947; Bigeleisen and Mayer, 1947; Kieffer, 1982). Other potentially isotope-dependent effects on lattice energy are ignored, since they are expected to be insignificant for moderate-mass elements (Schauble, 2011). Fractionation can be considered in terms of isotopic exchange reactions, which are driven thermodynamically toward equilibrium. Thus, isotopic equilibrium of one exchangeable atom, between two substances, AY and BY, can be described by an isotopic exchange reaction such as:

$$AY_l + BY_h = AY_h + BY_l \qquad (1)$$

where, Y_l and Y_h refer to the light and heavy isotopes of an element respectively. The isotope fractionation factor of the element Y between the substances AY and BY, α_{AY-BY}, is defined as the ratio of their isotope ratios. It can also be written as the ratio of the reduced partition functions (also called β-factors):

$$\alpha_{AY-BY} = \beta_{AY} / \beta_{BY} \qquad (2)$$

where β_{AY} is the isotopic fractionation factor of Y between the substance AY and a perfect gas of Y atoms (Richetet al., 1977).

The β-factors of each substance can be calculated from their harmonic vibrational frequencies (Méheut et al., 2007; Méheut et al., 2009; Blanchard et al., 2009) as following:

$$\beta_{AY}=[\prod_{i=1}^{3N_A}\prod_{\{q\}}\frac{\nu_{hq,i}}{\nu_{lq,i}}\frac{e^{-h\nu_{hq,i}/(2kT)}}{1-e^{-h\nu_{hq,i}/(2kT)}}\frac{1-e^{-h\nu_{lq,i}/(kT)}}{e^{-h\nu_{lq,i}/(2kT)}}]^{1/(N_qN)} \qquad (3)$$

where, N_A is the number of atoms in the unit-cell; N_q is the number of q-vectors in the Brillouin zone; N is the number of sites for the Y atom in the unit-cell;

$\nu_{lq,i}$ and $\nu_{hq,i}$ are the frequencies of the phonon with wavevector q and branch index i =1, $3N_A$, and the italic subscripts l and h mean the vibrational frequencies in AY with the light and heavy isotopes, respectively, T is the temperature, h is the Planck constant and k is the Boltzmann constant. In Eq. (3), the three translational modes at the center of the Brillouin zone, where $\nu^0_{lq,i} = 0$ and $\nu^0_{hq,i} = 0$, are not considered.

The β-factors were obtained from Eq.(3) using the phonon frequencies, $\nu_{lq,i}$ and $\nu_{hq,i}$, computed based on the density-functional perturbation theory (DFPT) (Baroni et al., 2001) and the linear response method. They were derived from the second-order derivative of the total energy with respect to atomic displacements. Pseudopotentials were generated using Vanderbilt's method (Vanderbilt, 1990). The generalized gradient approximation (GGA) proposed by Perdew et al. (1996) have been used for the exchange-correlation functional. Local density approximation (LDA) (Perdew and Zunger, 1981) was also used for the exchange correlation functional to calculate the crystal structures of the four minerals. Dynamical matrices were computed on regular q mesh and then interpolated in a dense q mesh to obtain the vibrational density of state of minerals. For all of the four minerals, the plane wave cutoff is set to be 50Ry and the Brillouin zones are sampled on $4\times4\times4$ meshes (Monkhorst and Pack, 1976). On the other hand, dynamical matrices are computed at $4\times4\times4$ q-vectors in the Brillouin zone. The effects of using the larger cutoff, K points and q points on the calculated properties are found insignificant.

Atomic relaxations were performed with the PWSCF code (Baroni et al., 2001; http://www.pwscf.org) until the residual forces on atoms became less than 10^{-4} Ry/a.u.

The cell parameters were also optimized.

Results and discussion

Crystalline structure

The pyrite-type structure has cubic structures and belongs to the space group $Pa\bar{3}$, and there are four formula units per unit cell. The primitive cell in our calculations includes 12 atoms. Its crystal structure is based on that of NaCl, where the Na and Cl sites are occupied by metals atom and S_2 dimers, respectively. In the pyrite-type structure, the metal atoms occupy the face-centered cubic lattice positions, and the sulfur atoms lie in pairs along the trigonal axes of the lattice, with each S located about three-eighths of the length of the diagonal from a metal atom (Berry et al., 1983). Each Fe atom is coordinated by six S atoms in a slightly distorted octahedron, and each S atom is tetrahedrally coordinated to three Fe atoms and one S atom.

The four minerals exhibit a rich diversity of magnetic properties: MnS_2 is an antiferromagnetic semiconductor (Hastings et al., 1959), FeS_2 is a nonmagnetic semiconductor (Antonov et al., 2008), CoS_2 is a ferromagnetic metal (Miyahara and Teranishi, 1968; Antonov et al., 2008), NiS_2 is an antiferromagnetic insulator (Antonov et al., 2008). So for MnS_2, CoS_2 and NiS_2, calculations were spin-polarized. In addition, for MnS_2 and NiS_2, calculations were set up to the antiferromagnetic, and for CoS_2 calculations were set up to the ferromagnetic structure. Magnetic moments were free to relax.

Our calculated structures of pyrite, cattierite, vaesite and hauerite are given in Table 1 together with experimental results. It is found that the calculated lattice

constants from GGA are closer to the experimental results. For pyrite, cattierite, vaesite and hauerite, our calculations by GGA underestimate the experimental lattice parameters by 0.2%, 0.4%, 1.1% and 0.7%; but the LDA underestimates the experimental lattice parameters by 2.4%, 3.4%, 3.7% and 2.5%. This indicates that our results based on GGA are in good agreement with experimental values (Brostigen and Kjekshus, 1969; Andresen et al., 1967; Nowack et al., 1991; Hastings et al., 1959). It is also found that the calculated interatomic distances by GGA are consistent with the available experiments much better. Therefore, GGA is a good exchange correlation for the structures and β-factors of the minerals.

Vibrational properties of pyrite

The number and symmetries of the Raman and infrared-active modes of pyrite have been determined using group theoretical methods (Lutz et al., 1974). The irreducible representations of the vibrations of pyrite are

$$\Gamma = A_g + E_g + 3T_g + 2A_u + 2E_u + 6T_u \qquad (4)$$

The gerade vibrations ($A_g + E_g + 3T_g$) are all active in the Raman spectrum and the ungerade vibrations are divided into the IR-active ($5T_u$) and optically inactive ($2A_u + 2E_u$) modes, plus the three acoustic modes. The harmonic phonon frequencies of pyrite, computed at the center of the Brillouin zone (Γ-point) using GGA, are shown in Table 2. There is good agreement between our calculated frequencies with the experimental data and previous DFT studies of the pyrite phase (Bührer et al., 1993; Blanchard et al., 2009; Spagnoli et al., 2010). The majority of the phonon frequencies are lower than the corresponding experimental values. In general,

theoretical frequencies underestimate by a few percents the measured infrared and Raman frequencies. This systematic error is typical of the GGA approximation.

Uncertainty in theoretical β-factors

Figure 1 shows the comparison of the three sets of computed phonon frequencies at the center of the Brillouin zone (Γ-point) of pyrite with experimental data. In the three sets of calculations, a good agreement with measurements can be obtained by a uniform scaling of the GGA frequencies. To quantify the scaling factor, we consider the slope of the best linear fit of our calculated points in Figure 1. The scaling factor is 1.028.

It found that a systematic correction of *n*% on the phonon frequencies induces a relative systematic correction on the logarithmic β-factors ($\ln\beta$) varying between *n*% (at low temperatures) and *2n*% (at high temperature) (Méheut et al., 2009). Therefore, a uniform scaling of +2.8% to the phonon frequencies of pyrite, is expected to induce a similar relative correction on $\ln\beta$ at maximum +5.6%. Since the fractionation ($\ln\alpha$) results from the difference of two logarithmic β-factors, a systematic error of 2.8% on all the phonon frequencies will lead to a relative error of at most 5.6% on the total fractionation. However, in the present study, we do not choose to apply any frequency correction, because there is an important uncertainty in the value of the applied scaling factors and we are not able to estimate analogous scaling factors for other minerals.

Concluding, errors arising from the computational approach (density-functional theory within the GGA approximation) are expected to the results in an

198 underestimation of the fractionation factors between 5 and 10% (Méheut et al., 2009).

199 **β-factors**

200 For sulfide minerals, the principal ratio of concern is $^{34}S/^{32}S$ (Seal, 2006). In the
201 present study, we only calculated the reduced partition function ratios of $^{34}S/^{32}S$
202 ($10^3\ln\beta_{34\text{-}32}$) in the range of 0-1000ºC. We fit the calculated data to least-squares
203 polynomial; a second power polynomial is sufficient to accurately fit the data over the
204 temperature range. Because mass-dependent isotopic fractionations vanish at infinite
205 temperature, the origin has been included as one of the points in the least-squares
206 analysis. The slope of the straight lines are listed in Table 3 and $10^3\ln\beta_{34\text{-}32}$ as a
207 functions of temperature are shown in Figure 2. We also show our calculated
208 $10^3\ln\beta$ data for pyrite, together with the previous theoretical calculations by Polyakov
209 et al. (2007) and Blanchard et al. (2009) in Figure 2. As shown in Figure 2, disparity
210 exists between the previous calculation, and our calculations are in between the
211 previous results. The apparent discrepancy for $10^3\ln\beta_{34\text{-}32}$ between our results and the
212 data of Blanchard et al. (2009), comes from the fact that in Blanchard et al. (2009) the
213 theoretical frequencies were multiplied by a scaling factor for determining the
214 β-factors but not in the present study. Otherwise, these two sulfur β-factors would
215 be in good agreement. As for Polyakov et al. (2007), the data must be revised
216 (Blanchard et al., 2012). The sulfur β-factor of Polyakov et al. (2007) is an indirect
217 estimation from the experimental heat capacity of pyrite and the iron β-factor that
218 they derived using Mössbauer measurements. The Mössbauer-derived iron β-factor
219 of pyrite has recently been revised leading to a good agreement with the DFT

220 iron β-factor (Blanchard et al., 2012; Polyakov et al., 2013). Therefore the sulfur
221 β-factor proposed by Polyakov et al. (2007) must also be revised. The
222 revised β-factor would be in better agreement with DFT results. $10^3 \ln \beta_{34\text{-}32}$ of all
223 minerals decrease dramatically with increasing temperature. The DFPT calculations
224 by us show that the order of heavy isotope enrichment is pyrite > cattierite > vaesite >
225 hauerite.

226 The factors that influence the magnitude of equilibrium stable isotope
227 fractionations are temperature, chemical composition, crystal structure and pressure
228 (O'Neil 1986). For the present discussion, pressure will not be discussed. The effect
229 of chemical composition on stable isotope fractionations depend most upon the nature
230 of the chemical bonds within the mineral (O'Neil 1977). And heavy stable isotope
231 fractionations in minerals depend principally on the nature of the bonds between the
232 atoms of an element and the nearest atoms in the crystal. So bonds with small
233 interatomic distances and thus large bond strengths, tend preferentially to incorporate
234 heavy isotopes (Zheng, 1995). In general, shorter bond lengths correlate with higher
235 reduced partition function ratios (Hill and Schauble, 2008).Also variations in $^{34}S/^{32}S$
236 distributions among coexisting sulfides are systematic and consistent with the relative
237 strengths of metal-sulfur bonds (Bachinski, 1969). As shown in Table 1, the
238 metal-sulfur distance increases in the order FeS_2, CoS_2, NiS_2 and MnS_2; but the
239 sulfur-sulfur distance decreases in the order FeS_2, CoS_2, MnS_2 and NiS_2. The two
240 sequences agree with the experimental results (Elliott, 1960) very well.
241 Sulphur-sulphur and metal-sulphur distances can give some indication of bond

242 strengths, shorter distances indicating larger bond strengths, the metal-sulfur bond
243 strength decrease in the sequence $FeS_2 > CoS_2 > NiS_2$, and sulfur-sulfur bond strength
244 increase in the sequence $FeS_2 < CoS_2 < NiS_2$ (Nickel et al., 1971). So according to our
245 results of the sulfur-metal bond length, the fractionation order would be pyrite >
246 cattierite > vaesite > hauerite. But according to our results of the sulfur-sulfur bond
247 length, the fractionation order would be pyrite < cattierite < vaesite < hauerite, and
248 this sequence is not consistent with the fractionation sequence of these four sulfides,
249 so the sulfur fractionation mechanism in disulfides is much complex and the effects of
250 sulfur-sulfur bond seems to be unclear. Nevertheless, there may be some errors for
251 Bachinski(1969) to estimate the sulfur-metal bond strength of NiS_2, CoS_2 and FeS_2,
252 and according to his estimates of the metal-sulfur bond strength sequence, the sulfur
253 isotope fractionation order would be $NiS_2 > CoS_2 > FeS_2$, which is opposite to the
254 results by us and Nickel.

255 The crystal structures can influence isotope fractionations to an extent depending
256 on how different the interatomic interactions are between the various structural forms,
257 and the heavy isotope apparently concentrates in the more closely packed or
258 well-ordered structures (O'Neil, 1977). Pyrite, cattierite, vaesite and hauerite have the
259 same structure (pyrite- type structure), and the unit cell volume increases through the
260 series $FeS_2 < CoS_2 < NiS_2 < MnS_2$. According to O'Neil, the heavy isotope apparently
261 concentrates in the more closely packed structures, the fractionation order would be
262 pyrite > cattierite > vaesite > hauerite.

263 In conclusion , our calculated reduced partition function ratios of pyrite, cattierite,

vaesite and hauerite are reasonable. It seems that the sulfur isotope fractionations mainly depend on metal-sulfur bond strength, and the effect that sulfur-sulfur bond strength on the sulfur isotope fractionations is unclear.

Implications

Our study shows that in pyrite-type disulfides, the variations of the metal-sulfur bond length are roughly out of accord with those of the sulfur-sulfur bond length. So the influence on sulfur isotope fractionation from sulfur-sulfur bond and metal-sulfur bond seems to be different according to the relationship of bond length, bond strength and the enrichment of heavy isotopes. And intuitively, the variation of metal atoms in disulfides makes the metal-sulfur bond length and sulfur-sulfur bond length different, and then results in the sulfur isotope fractionation among disulfides. In mineralogy, the pyrite group AX_2 is very complex, in which X may be S, Se, Te, As or Sb, and X_2 can be different atoms, such as FeS_2, CoS_2 and CoAsS. CoS_2 and CoAsS have different crystal structure, however CoS_2 and FeS_2 have the same crystal structure. So the impact on sulfur isotope fractionation caused by the substitution of metalloid element for sulfur seems to be much more complicated.

Disulfides can exist in most of metal sulfide deposit e.g. pyrite and arsenopyrite coexist in some gold deposits. Therefore, it seems to be useful for study of the ore deposits dealt with different disulfides to figure out the influence of the substitution of S by other metalloid element on the sulfur isotope fractionation, which is of particular interest in low temperature hydrothermal sulfide deposits.

Acknowledgments

This study was supported by funding from the National Science and Technology Planning Project (No.2011BAB03B09). We thank Huai Zhang, Tao Sun and Chunlin Deng for their valuable suggestions and help. We are very grateful to the Associate Editor Prof. Keith Refson and the two reviewers for their thoughtful and instructive reviews of this manuscript.

References

Andresen, A. F., Furuseth, S., and Kjekshus, A. (1967) On ferromagnetism of CoS_2. Acta Chemica Scandinavica, 21, 833.

Antonov, V. N., Andryushchenko, O. V., Shpak, A. P., Yaresko, A. N., and Jepsen, O. (2008) Electronic structure, optical spectra, and x-ray magnetic circular dichroism in CoS_2. Physical Review B, 78, 094409.

Bachinski, D. J. (1969) Bond strength and sulfur isotopic fractionation in coexisting sulfides. Economic Geology, 64, 56-65.

Balan, E., Cartigny, P., Blanchard, M., Cabaret, D., Lazzeri, M., and Mauri, F. (2009). Theoretical investigation of the anomalous equilibrium fractionation of multiple sulfur isotopes during adsorption. Earth and Planetary Science Letters, 284, 88-93.

Baroni, S., de Gironcoli, S., Dal Corso, A., and Giannozzi, P. (2001) Phonons and related crystal properties from density-functional perturbation theory. Reviews of Modern Physics, 73, 515-561.

Bente, K., and Nielsen, H. (1982) Experimental S isotope fractionation studies between coexisting bismuthinite (Bi_2S_3) and sulfur (S). Earth and Planetary Science Letters, 59, 18-20.

Berry, L. G., Mason, B. H., Dietrich, R. V. (1983) Mineralogy: concepts, descriptions, determinations. San Freeman, Francisco.

Bigeleisen, J., and Mayer, M. G. (1947) Calculation of equilibrium constants for isotopic exchange reactions. The Journal of Chemical Physics, 15, 261-267.

Blanchard, M., Poitrasson, F., Meheut, M., Lazzeri, M., Mauri, F., and Balan, E. (2009) Iron isotope fractionation between pyrite (FeS_2), hematite (Fe_2O_3) and siderite ($FeCO_3$): A first-principles density functional theory study. Geochimica et Cosmochimica Acta, 73, 6565-6578.

Blanchard, M., Poitrasson, F., Méheut, M., Lazzeri, M., Mauri, F., and Balan, E. (2012). Comment on "New data on equilibrium iron isotope fractionation among sulfides: Constraints on mechanisms of sulfide formation in hydrothermal and igneous systems" by VB Polyakov and DM Soultanov.Geochimica et Cosmochimica Acta, 87, 356-359.

Brostigen, G., Kjekshus, A. (1969) Redetermined crystal structure of FeS_2 (pyrite). Acta Chem Scand, 23: 2186-2188.

Bührer, W., Lafougere, E., and Lutz, H. (1993) Lattice dynamics of pyrite FeS_2 by coherent neutron scattering. Journal of Physics and Chemistry of Solids, 54, 1557-1565.

Craig, J. R., Vaughan, D. J., and Hagni, R. D. (1981) Ore microscopy and ore petrography. New York: Wiley.

Czamanske, G. K., and Rye, R. O. (1974) Experimentally determined sulfur isotope fractionations between sphalerite and galena in the temperature range 600□ to

275□. Economic geology, 69, 17-25.

Danielache, S. O., Eskebjerg, C., Johnson, M. S., Ueno, Y., and Yoshida, N. (2008). High-precision spectroscopy of ^{32}S, ^{33}S, and ^{34}S sulfur dioxide: Ultraviolet absorption cross sections and isotope effects. Journal of Geophysical Research: Atmospheres (1984–2012), 113, D17314.

Eiler, J. M., Bergquist, B., Bourg, I., et al. (2014). Frontiers of stable isotope geoscience. Chemical Geology, 372, 119-143.

Elliott, N. (1960) Interatomic distances in FeS_2, CoS_2, and NiS_2. The Journal of Chemical Physics, 33, 903-905.

Elcombe, M. M., and Hulston, J. R. (1975) Calculation on sulphur isotope fractionation between sphalerite and galena using lattice dynamics. Earth and Planetary Science Letters, 28, 172-180.

Farquhar, J., Bao, H., and Thiemens, M. (2000). Atmospheric influence of Earth's earliest sulfur cycle. Science, 289, 756-758.

Farquhar, J., and Wing, B. A. (2003). Multiple sulfur isotopes and the evolution of the atmosphere. Earth and Planetary Science Letters, 213, 1-13.

Grootenboer, J., and Schwarcz, H. P. (1969) Experimentally determined sulfur isotope fractionations between sulfide minerals. Earth and Planetary Science Letters, 7, 162-166.

Groves, D. I., Solomon, M., and Rafter, T. A. (1970) Sulfur isotope fractionation and fluid inclusion studies at the Rex Hill Mine, Tasmania. Economic Geology, 65, 459-469.

Guy, B. M., Ono, S., Gutzmer, J., Kaufman, A. J., Lin, Y., Fogel, M. L., and Beukes, N. J. (2012). A multiple sulfur and organic carbon isotope record from non-conglomeratic sedimentary rocks of the Mesoarchean Witwatersrand Supergroup, South Africa. Precambrian Research, 216, 208-231.

Halevy, I. (2013). Production, preservation, and biological processing of mass-independent sulfur isotope fractionation in the Archean surface environment. Proceedings of the National Academy of Sciences, 110, 17644-17649.

Hastings, J. M., Elliott, N., and Corliss, L. M. (1959) Antiferromagnetic Structures of MnS2, MnSe2, and MnTe2. Physical Review, 115, 13-17.

Hill, P. S., and Schauble, E. A. (2008) Modeling the effects of bond environment on equilibrium iron isotope fractionation in ferric aquo-chloro complexes. Geochimica et Cosmochimica Acta, 72, 1939-1958.

Hubberten, H. W. (1980) Sulfur isotope fractionations in the Pb-S, Cu-S and Ag-S systems. Geochemical Journal, 14, 177-184.

Kajiwara, Y., Krouse, H. R., and Sasaki, A. (1969) Experimental study of sulfur isotope fractionation between coexistent sulfide minerals. Earth and Planetary Science Letters, 7, 271-277.

Kajiwara, Y., and Krouse, H. R. (1971) Sulfur isotope partitioning in metallic sulfide systems. Canadian Journal of Earth Sciences, 8, 1397-1408.

Kieffer, S. W. (1982) Thermodynamics and lattice vibrations of minerals: 5. Applications to phase equilibria, isotopic fractionation, and high-pressure

thermodynamic properties. Reviews of Geophysics, 20, 827-849.

Kiyosu, Y. (1973) Sulfur isotopic fractionation among sphalerite, galena and sulfide ions. Geochemical Journal, 7, 191-199.

Li, Y., and Liu, J. (2006) Calculation of sulfur isotope fractionation in sulfides. Geochimica et Cosmochimica Acta, 70, 1789-1795.

Lutz, H. D., and Willich, P. (1974) Gitterschwingungsspektren. IX. Pyritstruktur. FIR-Spektren und Normalkoordinatenanalyse von MnS_2, FeS_2 und NiS_2. Zeitschrift für anorganische und allgemeine Chemie, 405, 176-182.

Macnamara, J., and Thode, H. G. (1950). Comparison of the isotopic constitution of terrestrial and meteoritic sulfur. Physical Review, 78, 307-308.

Méheut, M., Lazzeri, M., Balan, E., and Mauri, F. (2007) Equilibrium isotopic fractionation in the kaolinite, quartz, water system: Prediction from first-principles density-functional theory. Geochimica et Cosmochimica Acta,71, 3170-3181.

Méheut, M., Lazzeri, M., Balan, E., and Mauri, F. (2009) Structural control over equilibrium silicon and oxygen isotopic fractionation: a first-principles density-functional theory study. Chemical Geology, 258, 28-37.

Miyahara, S., and Teranishi, T. (1968) Magnetic properties of FeS_2 and CoS_2. Journal of Applied Physics, 39, 896-897.

Monkhorst, H. J., and Pack, J. D. (1976) Special points for Brillouin-zone integrations. Physical Review B, 13, 5188-5192.

Nickel, E. H., Webster, A. H., and Ripley, L. G. (1971) Bond strengths in the disulphides of iron, cobalt and nickel. The Canadian Mineralogist, 10, 773-780.

Nowack, E., Schwarzenbach, D., and Hahn, T. (1991) Charge densities in CoS2 and NiS2 (pyrite structure). Acta Crystallographica Section B: Structural Science, 47, 650-659.

O'Neil, J. R. (1986) Theoretical and experimental aspects of isotopic fractionation. Reviews in Mineralogy and Geochemistry, 16, 1-40.

O'Neil, J. R. (1977) Stable isotopes in mineralogy. Physics and Chemistry of Minerals, 2, 105-123.

Otake, T., Lasaga, A. C., and Ohmoto, H. (2008) Ab initio calculations for equilibrium fractionations in multiple sulfur isotope systems. Chemical Geology, 249, 357-376.

Perdew, J. P., Burke, K., and Ernzerhof, M. (1996) Generalized gradient approximation made simple. Physical review letters, 77, 3865-3868.

Polyakov, V. B., Clayton, R. N., Horita, J., and Mineev, S. D. (2007) Equilibrium iron isotope fractionation factors of minerals: reevaluation from the data of nuclear inelastic resonant X-ray scattering and Mössbauer spectroscopy. Geochimica et cosmochimica acta, 71, 3833-3846.

Polyakov, V. B., Osadchii, E. G., Chareev, D. A., Chumakov, A. I., and Sergeev, I. A. (2013). Fe β -factors for sulfides from NRIXS synchrotron experiments Goldschmidt. Mineralogical Magazine, 77, 1985.

Richet, P., Bottinga, Y., and Janoy, M. (1977) A review of hydrogen, carbon, nitrogen, oxygen, sulphur, and chlorine stable isotope enrichment among gaseous molecules. Annual Review of Earth and Planetary Sciences, 5, 65-110.

Rye, R. O., and Czamanske, G. K. (1969) Experimental determination of sphalerite-galena sulfur isotope fractionation and application to ores at Providencia, Mexico. In Geol. Soc. Am. Abstr 7, 195-196.

Sakai, H. (1968) Isotopic properties of sulfur compounds in hydrothermal processes. Geochemical Journal, 2, 29-49.

Salomons, W. (1971) Isotope fractionation between galena and pyrite and between pyrite and elemetal sulfur. Earth and Planetary Science Letters,11, 236-238.

Schauble, E. A. (2011) First-principles estimates of equilibrium magnesium isotope fractionation in silicate, oxide, carbonate and hexaaquamagnesium (2+) crystals. Geochimica et Cosmochimica Acta, 75, 844-869.

Seal, R. R. (2006) Sulfur isotope geochemistry of sulfide minerals. Reviews in mineralogy and geochemistry, 61, 633-677.

Smith, J. W., Doolan, S., and McFarlane, E. F. (1977) A sulfur isotope geothermometer for the trisulfide system galena-sphalerite-pyrite. Chemical Geology, 19, 83-90.

Spagnoli, D., Refson, K., Wright, K., and Gale, J. D. (2010) Density functional theory study of the relative stability of the iron disulfide polymorphs pyrite and marcasite. Physical Review B, 81, 094106.

Temmerman, W. M., Durham, P. J., and Vaughan, D. J. (1993) The electronic structures of the pyrite-type disulphides (MS_2, where M= Mn, Fe, Co, Ni, Cu, Zn) and the bulk properties of pyrite from local density approximation (LDA) band structure calculations. Physics and Chemistry of Minerals, 20, 248-254.

Urey, H. C., and Greiff, L. J. (1935) Isotopic exchange equilibria. Journal of the American Chemical Society, 57, 321-327.

Urey, H. C. (1947) The thermodynamic properties of isotopic substances. Journal of the Chemical Society (Resumed), 562-581.

Vanderbilt, D. (1990) Soft self-consistent pseudopotentials in a generalized eigenvalue formalism. Physical Review B, 41, 7892.

Vaughan, D. J., and Craig, J. R. (1978) Mineral chemistry of metal sulfides. Cambridge: Cambridge University Press.

Vaughan, D. J., and Lennie, A. R. (1991) The iron sulphide minerals: their chemistry and role in nature. Science progress, 75, 371-388.

Wang, K. (1989) Genetic mineralogy of the earth and Universe. Publishing House of Education in Anhui.

Wuensch, B. J., and Ribbe, P. H. (1974) Sulfide mineralogy . Mineralogical Society of Amer.

Zheng, Y. F., and Simon, K. (1991) Oxygen isotope fractionation in hematite and magnetite: A theoretical calculation and application to geothermometry of metamorphic iron-formations. European Journal of Mineralogy, 3, 877-886.

Zheng, Y.F. (1995) Oxygen isotope fractionation in TiO_2 polymorphs and application to geothermometry of eclogites. Chinese Journal of Geochemistry, 14, 1-12.

Figure captions

Figure 1. Comparison of experimental and theoretical vibrational frequencies. The dashed line is a linear fit to this study.

462 Figure 2. Comparison of reduced partition function ratios ($10^3 \ln \beta_{34\text{-}32}$) values for

463 pyrite, cattierite, vaesite and hauerite.

Table 1 Comparison of the calculated and experimental structure of pyrite, cattierite, vaesite and hauerite

Pyrite	This study -GGA	This study-LDA	Experimental[a]
a(Å)	5.405	5.287	5.418
V(Å^3)	157.902	147.784	159.044
Fe-S (Å)	2.255	2.204	2.262
S-S (Å)	2.189	2.165	2.177
Cattierite	**This study -GGA**	**This study-LDA**	**Experimental[b]**
a(Å)	5.506	5.341	5.528
V(Å^3)	166.920	152.359	168.929
Co-S (Å)	2.307	2.224	2.319
S-S (Å)	2.138	2.208	2.126
Vaesite	**This study -GGA**	**This study-LDA**	**Experimental[c]**
a(Å)	5.613	5.469	5.6765
V(Å^3)	176.842	163.578	182.912
Ni-S (Å)	2.365	2.297	2.394
S-S (Å)	2.073	2.081	2.074
Hauerite	**This study -GGA**	**This study-LDA**	**Experimental[d]**
a(Å)	6.054	5.946	6.097
V(Å^3)	221.885	210.220	226.646
Mn-S (Å)	2.568	2.525	2.590
S-S (Å)	2.097	2.044	2.087

a Brostigen and Kjekshus, 1969; b Andresen et al., 1967; c Nowack et al., 1991; d Hastings et al., 1959.

Table 2 Calculated and experimental frequencies of the transverse optical modes of pyrite (cm^{-1})

Mode	Active mode	Symmetry	Calculated[a]	Calculated[b]	This study	Experimental[c]
4		A_u	217	203	214	199
5-7	IR	T_u	220	215	215	215
8-9		E_u	244	236	240	225
10-12	IR	T_u	289	283	287	289
13		A_u	334	323	327	310
14-15	Raman	E_g	346	328	332	344
16-18	IR	T_u	348	331	339	343
19-21	Raman	T_g	351	341	343	344
22-23		E_u	371	355	361	396
24	Raman	A_g	372	359	363	382
25-27	IR	T_u	374	368	368	402
28-30	Raman	T_g	390	378	379	387
31-33	IR	T_u	395	387	390	407
34-36	Raman	T_g	430	427	421	433

a Blanchard et al. (2009); b Spagnoli et al. (2010); c Bührer et al. (1993)

Table 3 Fits of $10^3 \ln \beta$ based on the function $ax + bx^2$, with $x = 10^6 / T^2$ (T in K) for $^{34}S/^{32}S$ isotope fractionation

Mineral	Chemical formula	*a*	*b*
Pyrite	FeS_2	1.7702	-0.0075
Cattierite	CoS_2	1.2833	-0.0041
Vaesite	NiS_2	1.1458	-0.0036
Hauerite	MnS_2	0.9755	-0.0033

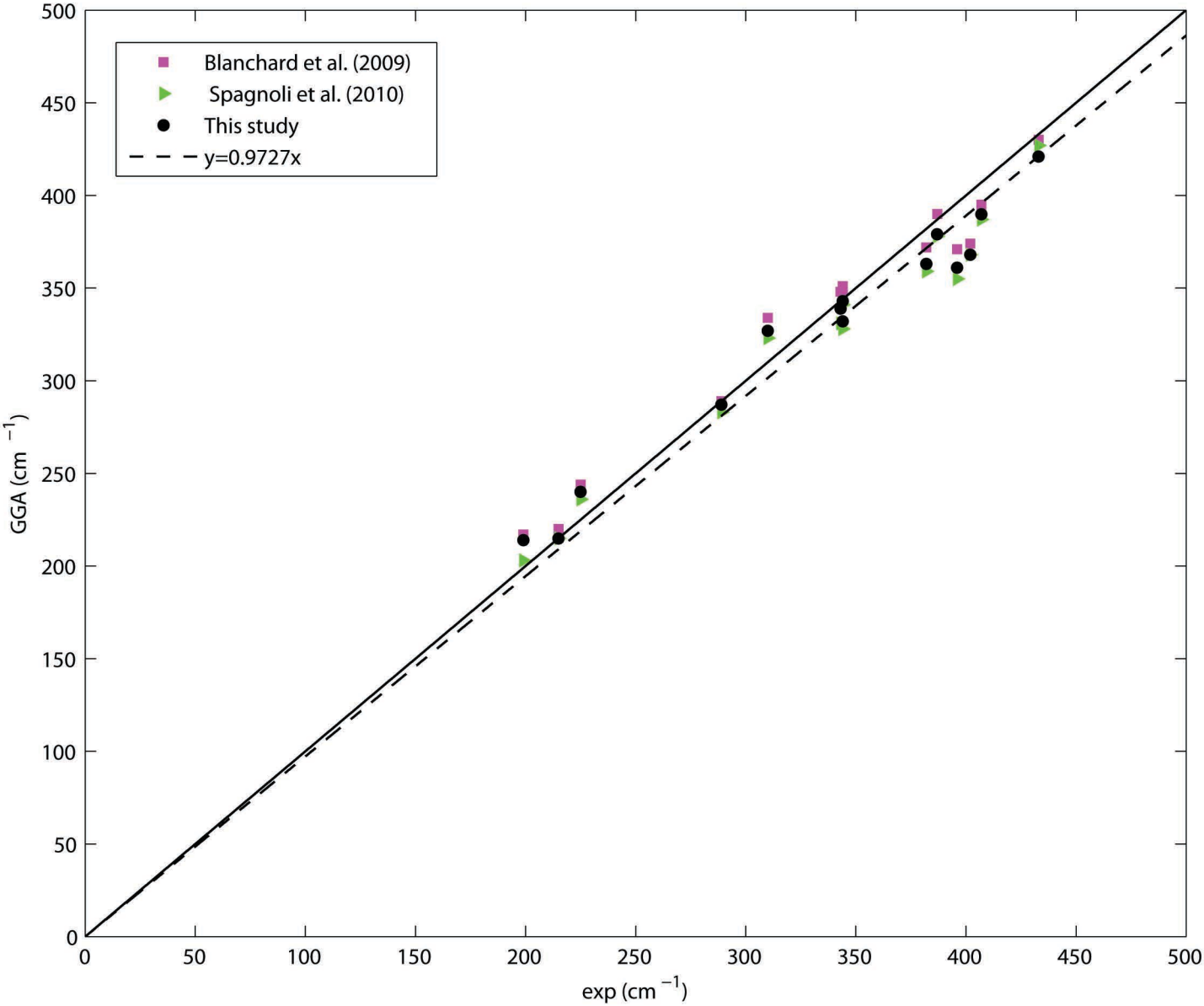
Blanchard et al. (2009)
Spagnoli et al. (2010)
This study
y=0.9727x
GGA (cm −1)
exp (cm −1)
0
50
100
150
200
250
300
350
400
450
500

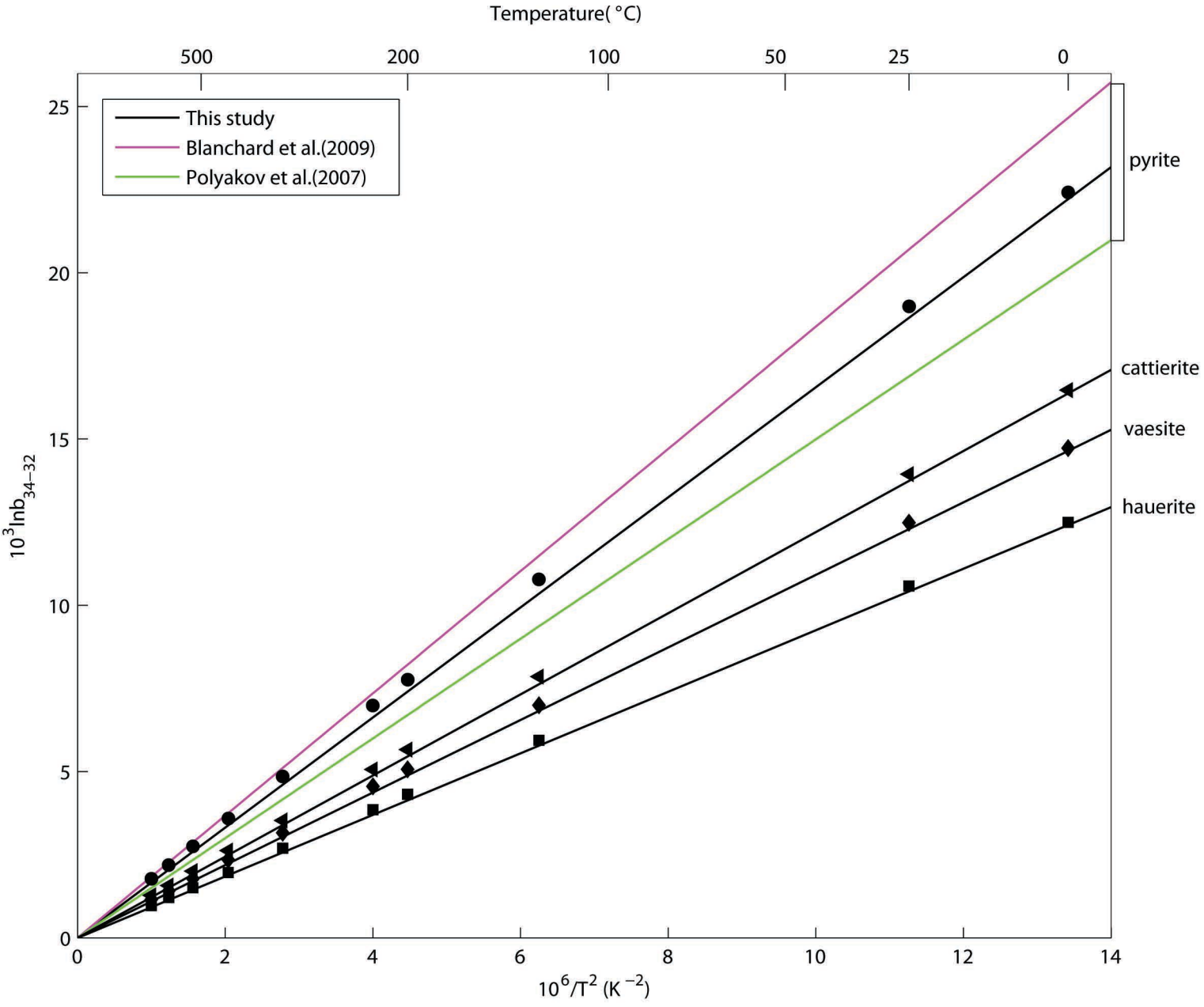
Temperature(°C)
500
200
100
50
25
0
This study
Blanchard et al.(2009)
Polyakov et al.(2007)
pyrite
cattierite
vaesite
hauerite
$10^3 \ln b_{34-32}$
$10^6/T^2$ (K $^{-2}$)
0
5
10
15
20
25
0
2
4
6
8
10
12
14